Space-Time Plasma-Steering Source: Control of Microwave Plasmas in Overmoded Cavities

V. Mazières, O. Pascal, R. Pascaud, L. Liard, S. Dap, R. Clergereaux, J.-P. Boeuf

Space-Time Plasma-Steering Source: Control of Microwave Plasmas in overmoded Cavities

V.Mazières,[1] O.Pascal,[1] R.Pascaud,[2] L.Liard,[1] S.Dap,[1] R.Clergereaux[1] and J-P.Boeuf[1]
[1] *Laboratoire LAPLACE, Université Paul Sabatier, 18 route de Narbonne, 31000 Toulouse France*
[2] *ISAE-SUPAERO, Université de Toulouse, France*

Recently, Space-Time Plasma Steering Source has been proposed as an innovative microwave plasma source to meet the challenge of controlling plasmas in overmoded cavities. This concept has been successfully demonstrated experimentally, allowing the space time control of nanosecond microwave plasmas on initiators. This paper gives insights into the path that shall be taken to reach full space-time control of plasmas in overmoded cavities. To that end, a key criterion, namely the "Plasma Steering criterion", is introduced and verified with a numerical model. This criterion must be respected for an accurate space-time control of plasmas in overmoded cavities. The importance of the plasma density (depending on its value with respect to the critical plasma density) on the plasma control capabilities is also highlighted.

CONTENTS

I. INTRODUCTION

One of the challenges that face plasma technologies is the development of "plasma source concepts that can be scaled to larger dimensions" [1]. Indeed, there is an increasing need to be able to process large area which comes, among other things, from the need to process solar panel, flat panel displays, and larger wafers [1]. Thus, a lot of efforts have been made toward the upscaling of existing technologies [2–6]. Furthermore, control of the deposition pattern of arbitrary shapes is also central to the development of many technologies, for example in the context of nanotechnologies [7] or for the fabrication of 3D metamaterials [8]. However, in material processing, all of these technologies share a common feature: the larger the surface to be processed, the more difficult it is to treat it. In fact, when increasing the area these technologies face physical and technological limitations [1, 9–11]. For microwave plasma sources, the inability to control plasmas comes from the overmoded nature of large cavities, which makes the control of the spatial distribution of the electric field (and thus of the plasma) very difficult with conventional technologies [12].

Another challenge facing plasma technologies is the development of plasma metamaterials, because their extension in three-dimensional structures will be of great interest in the future [1]. Indeed, plasmas have been proposed as a mean to develop reconfigurable metamaterials with exotic properties, such as nonlinearity or with negative refractive index when coupled with split ring resonators [13, 14]. More specifically, a certain spatial design of the system structure can be used to spatially pattern the medium properties. Very recently, an inverse design method has been proposed, allowing to determine the plasma pattern on a 2D plasma metamaterial (composed of plasma rods) giving the desired optical behavior, such as multiplexing or waveguiding [15]. However, the difficulties of controlling spatial plasma patterns have been pointed out in [16] and the authors state that in 3D coordinates, "formation methods of plasmas in arbitrary shapes are challenging research targets". Furthermore, these methods are not versatile as the spatial pattern obtained is limited by the spatially fixed structure of the system.

These two essential challenges come from the same issue: the difficulty of patterning plasma structures with arbitrary shapes in 2D and even more in 3D. To resolve this issue, a promising way is the innovative concept of microwave plasma source we introduced recently [17–20]. The idea of this source is to dynamically control the plasma location by changing the waveform of the transmitted signal to a large, overmoded cavity. This reverberant cavity allows to store the electromagnetic energy inside before focusing this energy at the desired instants and locations, in order to trigger breakdown phenomena (for low pressure plasmas, a metallic cavity is inherently present in the set-up). Following this principle, it is then the behavior of the waves inside the cavity that controls the plasma location. Thus, it allows a dynamic control of plasmas, hence the name "Space-Time Plasma Steering Source"[1] (STPSS). Experimentally, it has been shown to efficiently control plasmas on initiators in an overmoded cavity [17–19]. As noted in [20], the most essential step that needs to be taken for the development of this innovative plasma source is the "unhooking" of the plasmas from the initiators. This requires a precise understanding of the mechanisms at play. The aim of this paper is to provide a thorough investigation of these mechanisms in order to identify the key criterion allowing an efficient space-time control of plasmas with STPSS. A simple numerical model is used to verify the validity of this criterion. This paper is organized as follows:

In section II of this paper, the principle of the STPSS is presented and put into perspective with the principle of the usual microwave plasma sources based on microwave resonance. The general principle allowing space-time control of plasmas in overmoded cavities with STPSS is explained.

In section III, a key criterion, namely the "Plasma Steering Criterion", is introduced. It must be respected for envisioning an effective space-time control of plasmas by the STPSS. This criterion is then detailed for a particular case, namely the STPSS based on Time Reversal (TR).

In section IV, the model used to study the spatio-temporal control capabilities of STPSS is presented. It consists in coupling Maxwell equations with a fluid description of the plasma. The parameters of this model are set so that the physical conditions of the simulations are similar to the ones of the experimental plasmas that have been ignited by STPSS.

In section V, this model is used to investigate the validity of the "Plasma Steering Criterion" in the case of the STPSS based on TR. Description of a plasma ignition by TR is proposed when this criterion is respected or not. The influence of the initial plasma density on the space-time behavior of this unusual plasma is also investigated.

II. FROM MICROWAVE RESONANCE PLASMA SOURCE TO SPACE-TIME PLASMA STEERING SOURCE

Microwave plasma sources in cavities often use a resonance phenomena to reach an electric field high enough to obtain a gas breakdown. They are sometimes called "Microwave Resonance Plasma Source" (MRPS) [21]. However, as the volume of the cavity increases, the plasma control becomes more and more difficult, as explained in this section.

[1] Because of its potential application in the context of surface processing, it has been originally referred to "plasma brush" or "low pressure microwave plasma brush" [17–19], by analogy with the existing plasma brush based on plasma torch or plasma jet.

Sending a signal $s(t)$ to a cavity through a transmitter at a certain feeding location leads to a signal $r(t)$ measured by a receiver at a certain location inside the cavity, which can be written:

$$r(t) = s(t) * h(t) \tag{1}$$

with $h(t)$ the impulse response of the cavity with respect to these locations. In the spectral domain, equation (1) becomes:

$$R(f) = S(f).H(f) \tag{2}$$

with $R(f)$, $S(f)$ and $H(f)$ the complex Fourier transform of $r(t)$, $s(t)$ and $h(t)$, respectively. The transfer function $H(f)$ of the cavity results from the contribution of the resonant modes of the cavity, of frequencies f_k. It can be expressed as [22]:

$$H(f) = \sum_{k=1}^{M(f)} \gamma_k \Theta_k(f) \tag{3}$$

with $\Theta_k(f)$ the response of the k-th mode (with $k \in [\![1 : M(f)]\!]$), weighted by complex coefficients $\gamma_k = \alpha_k + j\beta_k$. At each of these modal responses $\Theta_k(f)$ is associated a certain spatial distribution of the eigenfield $\mathbf{E}_k(\mathbf{r})$. The modal weights γ_k are functions of the feeding and measuring positions and of the corresponding spatial field distribution $\mathbf{E}_k(\mathbf{r})$. At each frequency f, a certain number of modes $M(f)$, called "significant modes", contributes to the transfer function $H(f)$ [22, 23].

In the lossless case, the response of the modes $\Theta_k(f)$ becomes Dirac at frequencies $f = f_k$. The number of significant modes is thus equal to $M = 1$ and the transfer function can be written as $H(f) = \gamma_k^l(f)$, with $\gamma_k^l(f) = \gamma_k$ if $f = f_k$ and 0 otherwise. Feeding a cavity with a sinusoidal signal of frequency f_c equal to one of the mode frequencies leads to a spatial distribution of the field corresponding to the topography $\mathbf{E}_k(\mathbf{r})$ of the corresponding mode.

In a more realistic case, the presence of losses implies that energy is stored for a finite time in the cavity at resonance, resulting in a certain spectral width of the $\Theta_k(f)$ coefficients, noted Γ_k. The quality of a resonance is generally characterized by the quality factor of the cavity at the resonance frequency, defined as $Q_k = f_k/\Gamma_k$ [24]. It corresponds to the ratio between the stored energy and the dissipated energy (especially by the walls). As a first approximation, the stored energy is proportional to the inverse of the cube wavelength (the more the wavelength decreases and the larger the cavity becomes for the waves, the more energy is stored) and the dissipated energy is proportional to the inverse of the squared wavelength (since the energy is dissipated at the walls of the cavity). In these conditions the quality factor is proportional to the frequency f_k: $Q_k \propto (1/\lambda_k^3)/(1/\lambda_k^2) \propto 1/\lambda_k = f_k/c$. The spectral width must then be constant, as obtained experimentally in [25]. We will thus take $\Gamma_k = \Gamma$. These modal responses $\Theta_k(f)$ can generally be represented by Lorentzian functions, as shown for example in gray on the right of the schematic of Figure 1 for two cavities of different volumes.

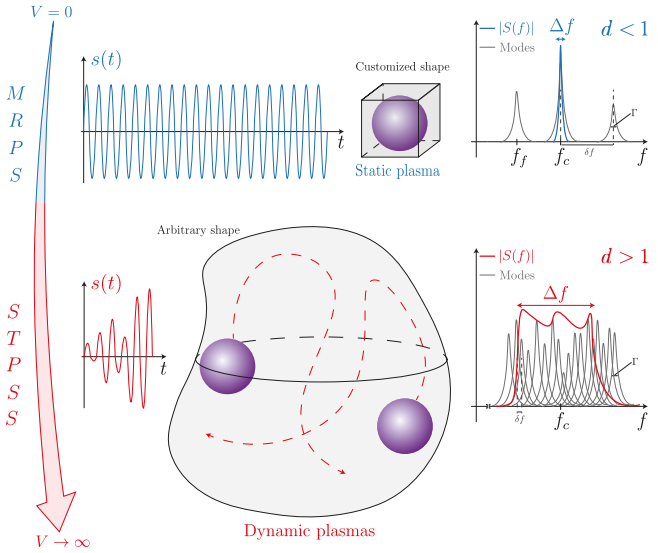

Figure 1. Control of microwave plasmas in cavities at a central frequency f_c as a function of the volume V of the cavity. For small volumes of the cavity, one single resonant mode can be excited (MRPS: Microwave Resonant Plasma Source). For large volumes space and time control of the plasmas is possible (STPSS: Space-Time Plasma Steering Source) by using transient signals.

Mathematically, equations (2) and (3) state that the measured signal $r(t)$, obtained by transmitting a signal $s(t)$ of central frequency f_c to the cavity, results from the contribution of a certain number of modes $M(f_c)$, called "significant modes". They correspond to the modes whose frequency f_k is close enough to the excitation frequency f_c to have a significant influence on the transfer function $H(f)$. Indeed, the modes that have a resonant frequency too far from f_c are negligible. In a simple way, these significant modes can be quantified by a dimensionless parameter d, called the mean modal overlap, defined by:

$$d = \frac{\Gamma}{\delta f} \tag{4}$$

where δf represents the average spacing between the resonance frequencies of the modes.

There are three regimes of modal overlap, which depend on the losses (*i.e.* of Γ) and the mean spacing between the frequencies of the modes δf. The latter depends on the feeding frequency for a given cavity volume or the cavity volume for a given feeding frequency. For pedagogical reasons, we focus on the latter case in this demonstration (a similar reasoning can be made with the former one), meaning we describe the microwave sources that can be used at a certain central frequency f_c as a function of the cavity volume V or equivalently of the

modal overlap d (indeed, for a constant frequency f_c, an increase of the cavity volume leads to an increase of the modal overlap).

II.1. Undermoded regime: Microwave Resonance Plasma Source

For small cavities (*i.e.* when the frequency f_c is close to the fundamental frequency f_f of the cavity), the frequencies of the modes are far apart from each others ($d < 1$) and the modes can be seen as independent of each other, as represented on the upper spectral diagram of Figure 1. The modal overlap is then small and the cavity is said to be undermoded. The cavity response $\mathbf{E}(\mathbf{r}, f)$ resembles the lossless response: $\mathbf{E}(\mathbf{r}, f) \propto \mathbf{E}_k(\mathbf{r})$ if $f = f_k$ and $\mathbf{E}(\mathbf{r}, f) \approx 0$ otherwise. Feeding the cavity with a sinusoidal signal of central frequency f_c equal to one of the frequency mode f_k leads to a spatial distribution of the field very similar to that of the corresponding eigenfield $\mathbf{E}_k(\mathbf{r})$.

Thus, in this regime, it is possible to excite only one resonant mode in order to obtain a spatial distribution of the electric field allowing a plasma at a desired location. To that end the spectral bandwidth Δf of the feeding signal $s(t)$ must be lower than the spectral width Γ of the excited mode. The resonance phenomenon can then be used to ignite plasmas and the plasma source is called MRPS. However, the presence of a plasma has an impact on the spatial distribution of the electric field. Thus, it is crucial to take this effect into account in order to avoid parasitic discharges. They can be avoided by a thorough design of the cavity, as stated in [21]: "The geometry of a resonant cavity is the key element in the design of the MRPS". The final cavity design is thus the result of many designing steps, usually done using a multi-physical model as for example done in [26].

Finally, feeding the final customized cavity with a sinusoidal signal oscillating at the proper frequency f_c leads to the desired spatially fixed plasma pattern, as represented on Figure 1. This source principle is effective for controlling plasmas in cavities as long as it is possible to excite one single resonant mode. It is thus limited to small cavities (compared to the excitation wavelength).

II.2. Moderate regime: Microwave Resonance Plasma Source and Space-Time Plasma Steering Source

For medium cavities, the modal overlap is moderate ($d \sim 1$). That is, the spectral spacing between modes is of the order of the spectral width of the modes $\delta f \approx \Gamma$. The cavity response to a sinusoidal signal of central frequency f_c equal to one of the frequency mode f_k is different from the corresponding lossless response $\mathbf{E}_k(\mathbf{r})$, as several modes (the ones with frequencies close to the feeding frequency f_c) contribute to the resulting field. The spatial distribution of the field is thus a combination of the eigenfields $\mathbf{E}_k(\mathbf{r})$ from which the frequency is close to the feeding frequency.

Thus, in this regime, controlling the spatial distribution of the field by feeding a resonant mode is complicated. Indeed, the central frequency f_c of the source must be finely tuned to excite only the desired mode and its spectral width must be lower than the one of the mode. Other solutions have been proposed, consisting in carefully designing the system such as several resonant modes (typically two or three) are obtained at the same resonant frequency. Then, the control of the spatial distribution of the field (and of the plasma) is done by exciting the cavity at this frequency, resulting in the simultaneous exciting of these resonant modes[2] [27–29]. To avoid parasitic discharges in the cavity, a quartz dome delimiting the plasma chamber (of volume much lower than the one of the cavity) may also be placed inside the cavity [28]. For those sources, the designing process of the system (cavity + coupling devices + quart windows) requires even more accuracy than for the undermoded regime.

To control the spatial distribution of the field inside the cavity in this regime, another solution consists in using feeding signals $s(t)$ with bandwidth much larger than the modal bandwidth Γ. We called this method of space-time plasma control "Space-Time Plasma Steering Source", operating in this regime (moderate) and in overmoded regime. Its principle is detailed in the following subsection.

II.3. Overmoded regime: Space-Time Plasma Steering Source

For large cavities (compared to the excitation wavelength), the spacing between modes is smaller than the width of the modes ($d > 1$), so the modal overlap is strong. The modes overlap each other (as represented on the lower spectral diagram of Figure 1) and the response $\mathbf{E}(\mathbf{r}, f)$ to an excitation depends on a large number of modes. The number of significant modes is important. In this case the spatial distribution of each eigenfield is not important and the resulting field can be assimilated to a random superposition of plane waves. In this regime, feeding only one resonant mode is difficult if not impossible [12]. It follows that the control of plasmas in this regime is not possible with conventional MRPS.

The control of plasmas in large cavities thus requires the development of different methods. A promising one is the STPSS we introduced recently. Instead of controlling the spatial distribution of the field and thus of

[2] These sources have been referred to as "multimode" sources [27, 28], because several modes are simultaneously excited. However, for the same reason, they have also been referred to as "overmoded" [29], which in this case does not have the same signification as the one used in the present paper (in which it corresponds to a modal regime of overlap).

the plasma by carefully shaping the cavity geometry, dynamic control of plasma distribution is made possible by shaping the temporal waveform of the transmitted signal to the cavity. The waveform of this signal determines the spatio-temporal behavior of the waves inside the cavity.

For a dynamic control of the spatial distribution of the field in the cavity, the spectral bandwidth Δf of the transmitted signal $S(f)$ must be significantly larger than the spectral width of the modes Γ. Then, the amplitude and the phase of $S(f)$ must be tuned in order to excites the cavity modes (contained in $H(f)$) in such a way that the desired space-time field is obtained in the cavity. Indeed, when transmitting the signal $S(f)$ to the cavity, the amplitude and phase of $S(f)$ weights the complex modal weights γ_k as stated by equation (2). With a large enough number of modes in the useful bandwidth Δf, astutely weighting these modal weights leads to a space-time control of the field in the cavity.

In other words, shaping the temporal waveform of $s(t)$ – or equivalently controlling the amplitude and the phase of the excited modes in the bandwidth Δf – allows a control of the behavior of the waves in the cavity. Then, these waves can be structured so that, by interference, a local concentration of electromagnetic power occurs at desired location and instant. If this concentrated energy is high enough, a breakdown phenomena can be triggered at this instant and location. Following this idea, shaping the waveform of $s(t)$ allows a spatio-temporal control of plasmas in overmoded cavities, as represented on Figure 1. *Thus, this waveform is the key element in the design of the STPSS.* In this case, plasmas are ignited with transient signals. Space-time steering of plasmas is then made possible in a pulsed regime.

STPSS offers the possibility of space-time control of plasmas in cavities as long as there are enough modes contained in the bandwidth of the feeding signal. It is thus limited to large cavities (and medium ones). Furthermore, it does not require a fine tuning of the system design.

III. THE "PLASMA STEERING CRITERION"

In the case of plasma control by STPSS, the cavity is excited by transient signal. The temporal waveform of this signal determines the behavior of the wave in the cavity. In order to obtain a concentration of energy at the desired instant t_p and location $\mathbf{r}_p$, waves must propagate during a certain amount of time preceding this instant. Furthermore, after the concentration of energy is desired, waves will continue to propagate during a certain duration inside the cavity. Thus, igniting a plasma with the STPSS requires the presence of the waves inside the cavity during a certain duration, that we call τ_e. The aim is then to obtain at the desired instant t_p and location $\mathbf{r}_p$ an electric field high enough to trigger a breakdown phenomena.

To define breakdown, the continuity equation can be written as (without attachment and neglecting recombination) [30, 31]:

$$\ln \frac{n_e}{n_{e_0}} = \int_0^t \nu_{net}\, dt \tag{5}$$

with $\nu_{net} = \nu_i - \nu_d$ the net ionization coefficient, ν_i the ionization rate, ν_d the diffusion rate, n_{e_0} the initial density of electrons and where the microwave power is assumed to be turned on at $t = 0$.

The critical multiplication beyond which one considers that there is breakdown is generally (and quite empirically) taken equal to $n_e/n_{e_0} = 10^8$ [30, 31]. For a rectangular shape of the microwave power, applied during τ_b, breakdown condition reduces simply to [30, 31]:

$$\nu_{net} = \frac{\ln 10^8}{\tau_b} \tag{6}$$

According to this criterion, for a rectangular shape of the microwave power, a breakdown occurs when the electric field reaches the breakdown value E_b, at which $\tau_b \nu_{net} \approx 20$.

For triggering a breakdown only at the desired instant t_p and location $\mathbf{r}_p$, the value of the electric field E_p at this instant and location must be equal or superior to the value of the breakdown field and no breakdown should occurs before and after this instant anywhere in the cavity. Breakdown is a transient phenomenon, whose characteristics have been shown to depend, among other things, on:

- The duration of the applied field [30], as can be seen in equations (5) and (6): $E_b = E_b(\tau_b)$. The longer this time, the lower the field level required to break down the gas [30, 32].
- The shape of the microwave pulse [30, 31, 33].

This dependence of the breakdown field on these two parameters is central in the determination of the criterion allowing an accurate space-time steering of plasmas by STPSS. In the following of this section, this criterion is introduced in the general case and then in the particular case of the STPSS based on TR.

III.1. Introduction of the "Plasma Steering Criterion"

The principle of space-time plasma control by STPSS is illustrated on Figure 2. A representation of an arbitrary temporal evolution of the magnitude $|s(t)|$ of the transmitted signal to the cavity is represented. The shape of this waveform must allows a concentration of energy high enough at the desired instant t_p and location $\mathbf{r}_p$ so that a plasma is ignited and at the same time an energy low enough anywhere in the cavity so that no breakdown occurs anywhere else in the cavity. Three signals are measured in the cavity, two of them at random locations $\mathbf{r}_g$ and $\mathbf{r}_y$ (represented in green and yellow respectively)

and one at the location $\mathbf{r}_p$ at which a plasma is desired. The electric fields at the locations of the corresponding receivers are linked to theses measured signals through the transfer function of the receivers. For simplicity, we will focus in the following of this section on these electric fields, assuming a similar evolution between these electric fields and the measured signals.

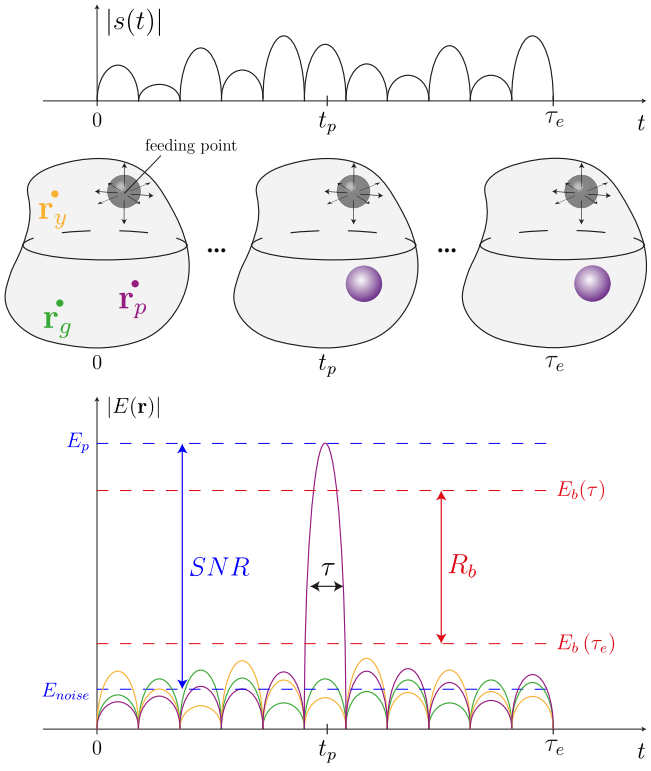

Figure 2. Schematic of a space-time plasma control by STPSS. Illustration of the "Plasma Steering Criterion".

The evolution of the two electric fields at $\mathbf{r}_g$ and $\mathbf{r}_y$ in the cavity are plotted in green and yellow on Figure 2, respectively. On these signals, the levels of the fields evolve around a mean value E_{noise}. The evolution of the electric field at location $\mathbf{r}_p$ is represented in purple. Before the instant t_p, at which a breakdown is desired, the mean level of the noise field is the same as elsewhere in the cavity, meaning equal to E_{noise}. At the instant t_p, the level of the field at this location $\mathbf{r}_p$ increases significantly during a duration τ. If this field reaches the breakdown value $E_b(\tau)$ corresponding to a duration of application of the field of τ, a breakdown occurs at instant t_p and location $\mathbf{r}_p$, as represented on Figure 2. In order to avoid parasitic discharges at any time anywhere in the cavity, the mean level of the noise E_{noise} must be lower than the breakdown field $E_b(\tau_e)$ corresponding to a duration of application of the field of τ_e, as represented on Figure 2.

Thus, for an accurate control of plasmas: $E_p \geqslant E_b(\tau)$ and at the same time $E_{noise} < E_b(\tau_e)$. This discussion allows to determine the key criterion for an accurate control of plasmas by TR, which is contained in the following expression:

$$SNR > R_b \tag{7}$$

with $SNR = E_p/E_{noise}$ defined as the ratio between the level of the field at the breakdown instant t_p and the mean level of the noise, and $R_b = E_b(\tau)/E_b(\tau_e)$ defined as the ratio between the breakdown level for a duration τ and the breakdown level for a duration τ_e, as represented on Figure 2. Relation (7) must be satisfied together with $E_p \geqslant E_b(\tau)$ or $E_{noise} < E_b(\tau_e)$.

We call this criterion the "Plasma Steering Criterion", as when this criterion is met, an effective space-time control of plasmas can be envisioned (note that, as shown in simulation in section V, the quality of this control is also conditioned by the value of the maximum plasma density with respect to the critical plasma density). In the following subsection, this criterion is detailed for the STPSS based on Time Reversal.

III.2. The "Plasma Steering Criterion" for the Space-Time Plasma Steering Source based on Time Reversal

As explained in section II.3, the temporal waveform of the signal $s(t)$ is the key element in the design of the STPSS. Several techniques can be envisioned to construct this signal so that its emission in the cavity, described by equation (1), yields the desired space-time evolution of the field, meaning a field meeting the "Plasma Steering Criterion". Experimentally, we have used two techniques to construct this signal $s(t)$: Time Reversal [17, 18] and Linear Combination of Configuration Field [19]. The latter one have been shown to enhance spatial control of plasmas compared to the former one, but is more complicated to implement as it requires more complex signal processing developments. For simplicity, we focus on the present paper on the STPSS based on TR.

The spatio-temporal patterning of plasmas in overmoded cavities based on TR requires two steps. The first step consists in measuring, using a transducer array named Time Reversal Mirror (TRM), one (or several) impulse response $i(t)$ in the cavity. This impulse response corresponds to the cavity response to an initial impulsion $e(t)$ of duration τ, defined here as the duration at half maximum. It can be expressed as $i(t) = e(t) * h(t)$. The level of this signal decreases exponentially, due to the losses in the cavity. The duration of this exponential decay is usually characterized by the reverberation time, that we call τ_r.

Time reversed of this impulse response $s(t) = i(-t)$ is then transmitted to the cavity by the TRM. Assuming system reciprocity ($h(t) = h(-t)$) [34], the signal $r(t)$ measured at location $\mathbf{r}_p$ is [35]:

$$r(t) = i(-t) * h(t) = e(-t) * h(-t) * h(t) \tag{8}$$

This equation reflects a focusing of the waves. Indeed, sending $i(-t)$ leads to a coherent summing of these waves

at the focusing instant t_p and location $\mathbf{r}_p$, focusing of duration equal to the one of the initial impulse τ. Analytically, this process can be highlighted by rewriting equation (8) as [22]:

$$r(t) = \rho e(-t) + n(t) \tag{9}$$

with $\rho e(-t)$ the component of $r(t)$ that is coherent with respect to $e(-t)$ (*i.e.* the TR focusing peak) and $n(t)$ a residual noise. Obtaining this coherent component is related to the phase of the transmitted signal $S(f)$ (corresponding to the time reversed impulse response) that exactly compensates the phase of the modes (argument of the modal weights γ_k). Indeed, in the spectral domain, equation (8) writes $R(f) = |H(f)|^2.|E(f)|.e^{-j\phi_E(f)}$ with $|E(f)|.e^{-j\phi_E(f)}$ the Fourier transform of $e(-t)$. The phase of the received signal $R(f)$ is thus equal to the inverse of the phase $\phi_E(f)$ of the initial impulse. This reflects the coherent summing of the waves at the focusing instant and location. The presence of noise $n(t)$ surrounding this focusing peak is related in the spectral domain to the non-flat nature of the transfer function $H(f)$ (due the presence of resonant modes), that induces a difference between the magnitude $|R(f)|$ of the received signal and the one of the initial pulse $|E(f)|$. In the temporal domain, this is equivalent to saying that before and after the focusing (and elsewhere in the the cavity), the waves are incoherently summed. Thus, the signal measured at the focusing location possesses a focusing peak ($\rho e(-t)$) and surrounding noise ($n(t)$) before and after.

The evolution of the electric field $E_{TR}(t)$ at $\mathbf{r}_p$ is linked to the measured signal $r(t)$ through the transfer function of the receivers. As done in section III.1, we will focus in the following of this section on the electric field, assuming a similar evolution between $E_{TR}(t)$ and $r(t)$.

It follows that the electric field $E_{TR}(t)$ measured at the focusing location possesses a focusing peak and surrounding noise before and after. If the focusing field E_p is high enough, a breakdown occurs at the focusing instant t_p and location $\mathbf{r}_p$, as represented on Figure 3. In the case of the STPSS based on TR, the signal transmitted to the cavity allowing for an accurate space-time control of plasmas corresponds to the time reversed impulse response, meaning $s(t) = i(-t)$.

One important parameter used to characterize the TR performance is the signal-to-noise ratio SNR [36, 37], defined as:

$$SNR = \frac{\langle E(\mathbf{r}_p, t_p)\rangle}{\langle E(\mathbf{r}_p, t \notin \tau)\rangle} = \frac{\langle E_p\rangle}{\langle E_{noise}\rangle} \tag{10}$$

where the brackets $< . >$ denote an ensemble average and E_{noise} the rms value of $\langle E(\mathbf{r}_p, t \notin \tau)\rangle$ [36–40]. In a chaotic cavity[3], the spatial signal-to-noise ratio, defined as $SNR_{spatial} = E_p/E_{noise}^{spatial}$ with $E_{noise}^{spatial} = \langle E(\mathbf{r} \neq V_p, t_p)\rangle$ (with V_p the focusing volume), has been shown to be equivalent to the temporal signal-to-noise ratio: $SNR_{spatial} = SNR$ [39]. In this case, a measurement of the temporal evolution of the electric field at one location in the cavity during a TR experiment is an image of the field level elsewhere in the cavity. Since the introduction of Time Reversal in the 90s [41], a lot of work has been done on understanding the parameters influencing this SNR [35, 37, 38]. The square of this signal-to-noise ratio SNR^2 has been shown to be proportional to Δf and the number N_{ant} of transducers in the TRM. Furthermore, it is proportional to the reverberation time τ_r in the overmoded case ($d > 1$) and to the Heisenberg time τ_H (that depends on the cavity volume) in the undermoded case ($d < 1$).

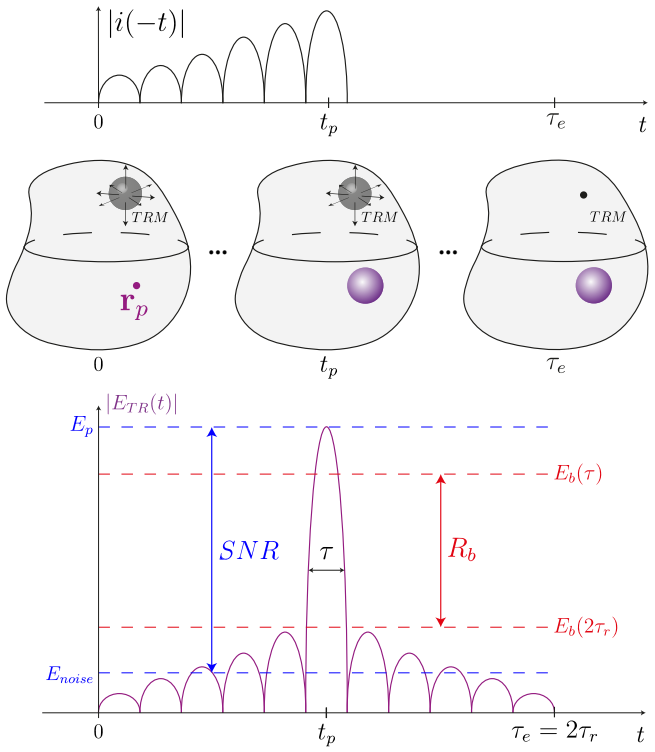

Figure 3. Schematic of a space-time plasma control by STPSS based on TR. Illustration of the corresponding "Plasma Steering Criterion".

In a TR operation the level of the field exponentially increases before the focusing peak, with a duration classically equal to the reverberation time τ_r. After the focusing peak, the waves continue to propagates and follow an exponential decay, during a duration of τ_r. Thus, precise evaluation of the breakdown condition for the noise surrounding the peak would require taking into account the exponential growth and decay shapes. For simplicity, we consider, as a first approximation, that the exponentially increasing then decreasing shape of the electric field in the cavity is equivalent, with respect to the breakdown, to a constant level of the field of its rms value E_{noise}. Following this idea, for an accurate control of plasmas

[3] In short, a chaotic cavity ensures, statistically, a uniform spatial distribution of the field, avoiding undesired energy concentrations that would compromise an efficient spatial focusing by TR at the desired location.

by TR, it is required that $E_p \geqslant E_b(\tau)$ and at the same time $E_{noise} < E_b(2\tau_r)$, as represented on Figure 3. Thus for the STPSS based on TR, the "Plasma Steering Criterion" becomes:

$$SNR > R_b = \frac{E_b(\tau)}{E_b(2\tau_r)} \tag{11}$$

with R_b defined as the ratio between the breakdown level for a duration τ and the breakdown level for a duration $2\tau_r$. When this criterion is met, an accurate control of plasmas by STPSS based on TR can be envisioned, as shown in simulation in section V, using the model presented in section IV.

IV. MODEL PRESENTATION

The aim of the model presented in this section is to describe plasma ignition by STPSS based on TR. The simulation conditions are chosen so that they are close to the experimental TR plasmas. The only experimental demonstrations of these plasmas are our recent works, in which the plasmas are ignited on initiators in argon at a pressure close to $p = 1.5$ torr [17, 18]. As a result, the details of the physical mechanisms of these plasmas are not fully understood yet, and more experimental characterization are necessary, as noted in [18]. We focus in the present paper on making use of a simple physical model to verify the validity of the "Plasma Steering Criterion". Developing a more accurate physical model is beyond the scope of this paper.

Experimentally, these plasmas have been ignited in argon and the minimum breakdown field has been found around $p = 1.5$ torr [18]. The same conditions (argon and pressure) are chosen for the simulations presented in this paper. Furthermore, experimentally, the presence of initiators locally enhance the electric field at the focusing locations and play an significant role on the plasma dimensions, as noted in [18]. This experimental plasma dimension was found to be typically of radius $L = 5$ mm [18]. In the present paper, in simulation, we focus on a more "ideal" case, where the breakdown field is reached only as a consequence of the focusing of the waves by TR, without the need of initiators. Hence, the plasma dimension in simulation will be equal to the focusing dimension, meaning of half the wavelength. Finally, experimentally, TR plasmas have been maintained in a pulsed regime. In the present paper, we focus on one plasma ignition by TR, as the aim is verifying the validity of the "Plasma Steering criterion". A description of a pulsed regime would require a more elaborated model than the one used in this paper because it requires an accurate description of the plasma decay between pulses, which is outside the scope of this paper. Future work is planned on the description of this pulsed regime.

A 2D simulation is used for computational time considerations. The cavity in which the plasmas are controlled by TR is a truncated disk with reflecting lossy walls, as represented on Figure 4. It is a chaotic cavity, which has been shown to enhance the space-time TR focusing capabilities [36, 38]. We focus in this paper on the Transverse Electric (TE) case, meaning the electric field is along the z axis and the magnetic field is contained in the xy plane. The same central frequency and pulse duration as for the experimental demonstration of plasma ignition by TR [17, 18] is chosen in simulation, meaning a central frequency of $f_c = 2.4$ GHz and a pulse duration of $\tau = 4$ ns, τ being here the duration at half maximum. The corresponding bandwidth associated to this pulse is of $\Delta f = 250$ MHz. The dimensions and the wall losses of the cavity are chosen so that its modal overlap is similar to the one of the experimental cavity in which plasmas have by ignited by TR [17, 18]. This gives a cavity surface of $S_{cavity} = 3.5$ m^2 for a mean modal overlap of $d = 3.5$, meaning the cavity is overmoded. The walls conductivity is tuned to obtain a reverberation time equal to the experimental one, meaning of $\tau_r = 300$ ns (here the reverberation time is defined as the double of the inverse of the spectral width of the modes: $\tau_r = 2/\Gamma$, with $\Gamma \approx 6$ MHz, the presence of a factor 2 being a consequence of the signals modulation at the carrier frequency f_c).

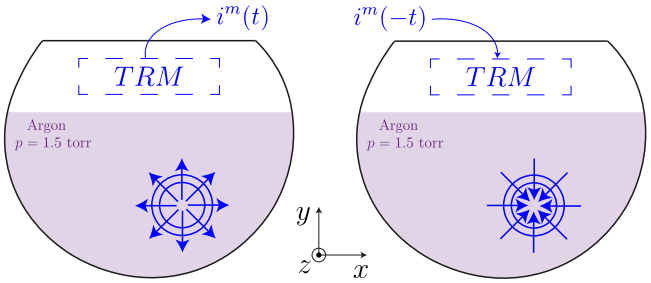

Figure 4. Schematic of the two steps of the TR operation. The region where the TRM (Time Reversal Mirror) is located (in white) is at atmospheric pressure (no plasma can develop) and the plasma chamber (in purple) is at a pressure $p = 1.5$ torr. (Left) Measure of the impulse responses $i^m(t)$ by a certain number of transducers in the TRM, $m \in [\![0 : N_{ant}]\!]$. (Right) Emission of the time reversed impulse responses $i^m(-t)$ by the TRM.

Experimentally, TRM, consisting of one emitting monopole, is located in an appendix of the cavity in which the initial air remains at atmospheric pressure to prevent gas breakdown in its vicinity during the high power reemission of the time-reversed waveforms [17–19]. For the same reason, in simulation the fluid model is resolved only on the bottom part of the cavity (TRM is located on the upper part), coloured in purple on Figure 4.

The method used in simulation is the following. An initial plasma density n_{e_0} is assumed to be present in the lower part of the cavity (coloured in purple on Figure 4). Plasma ignition by TR in simulation consists in sending a initial pulse $i(t)$ of duration τ at the location at which a plasma is desired, this location being inside the bottom part of the cavity (in purple). The impulse responses $i^m(t)$ are measured by the TRM, with a certain number of receivers N_{ant}. Then, theses impulses re-

sponses are time reversed and transmitted by the TRM, leading to a focusing of duration τ at the desired location, as represented on Figure 4. The amplitude of these time reversed impulse responses $i^m(t)$ is then adjusted so that the plasma density at the focusing location increases with a factor of 10^8, reflecting the presence of a plasma breakdown at this location.

The receivers and transmitters are assumed to be ideals in simulation, meaning excitation of the cavity is done by imposing an electric field at the desired locations and the measured signals ($i^m(t)$ and $r(t)$) are in volt per meter. It follows that, for example during the second phase of TR, the electric field at $\mathbf{r}_p$ is equal to the measured signal: $E_{TR}(t) = r(t)$. Thus, in section V showing the simulation results, we only talk about $E_{TR}(t)$.

IV.1. Physical model

Maxwell equations are coupled with the plasma transport equations through the electron current density, as in [42, 43] with an additional current density representing the wall losses:

$$\nabla \times \mathbf{E} = -\mu_0 \frac{\partial \mathbf{H}}{\partial t} \tag{12}$$

$$\nabla \times \mathbf{H} = \varepsilon_0 \frac{\partial \mathbf{E}}{\partial t} + \mathbf{J}_p + \mathbf{J}_c \tag{13}$$

$$\mathbf{J}_p = -e n_e \mathbf{v}_e \tag{14}$$

with the simplified electron momentum transfer equation:

$$\frac{\partial \mathbf{v}_e}{\partial t} = -\frac{e\mathbf{E}}{m_e} - \nu_m \mathbf{v}_e \tag{15}$$

Here, $\mathbf{E}$ and $\mathbf{H}$ represent the electric and magnetic field respectively; $\mathbf{J}_p$ is the plasma current density induced by the waves (the ion contribution to the current density is neglected) and $\mathbf{J}_c = \sigma\mathbf{E}$ the density current representing the wall losses (with σ the wall conductivity). n_e is the electron density, $\mathbf{v}_e$ the electron mean velocity, ε_0 and μ_0 the permittivity and permeability of vacuum respectively. m_e represents the electron mass and ν_m the electron-neutral collision frequency in argon.

The electron mobility can be obtained from the electron-neutral momentum collision frequency by $\mu_e = e/(m_e\nu_m)$, the electron diffusion coefficient is given by $D_e = \mu_e k_B T_e/e$ and the ambipolar diffusion coefficient by $D_a = (\mu_i/\mu_e)D_e$, with $\mu_e/\mu_i = 100$. On the time scales we are considering here, electron diffusion can be neglected. The electron diffusion time can be estimated using the following equation: $\tau_{diff} = \Gamma^2/D_{diff}$ with D_{diff} being the free or ambipolar diffusion, depending on the value of the electron density, and L is the characteristic dimension of the plasma defined by the the dimension of the region of electromagnetic energy deposition. In the case of TR focusing, this dimension is of half the wavelength [44]. Consequently, L is set equal to $\lambda_c/2 \approx 6$ cm. As the aim of the simulations is to describe plasma ignition by TR, their duration is set to two times the reverberant time τ_r, as it allows the description of the exponential growth preceding the focusing peak and the exponential decay following this peak, as can be seen on Figure 3. The simulations duration is then equal to $\tau_e = 2\tau_r = 600$ ns, which is much shorter than the characteristic diffusion times (free and ambipolar): the free electron diffusion coefficient of $T_e = 2$ eV electrons in argon at 1 torr is about 50 m^2/s, so that the electron diffusion time L^2/D_{diff} is on the order of 100 μs.

Thus, diffusion can be neglected in our simulations (this has been checked numerically in the examples below) and the plasma density n_e can be described by a simple fluid equation accounting for plasma growth associated with ionization (without attachment and neglecting recombination and diffusion):

$$\frac{\partial n_e}{\partial t} = s_e = \nu_i n_e \tag{16}$$

with s_e is the net electron production rate and ν_i the ionization rate. The evolutions of ν_i and ν_m as a function of the value of the rms field E_{rms} are obtained with Bolsig + [45].

IV.2. Numerical model

These equations are discretized using Finite-difference time domain (FDTD) method. This method uses centered finite differences on a uniform Cartesian grid, yielding the spatio-temporal variation of the electric and magnetic fields and of plasma quantities [42, 43]. An issue encountered when making use of numerical modelling by FDTD is numerical dispersion. It is a consequence of the discretization of continuous functions (since they represent a physical quantity). It is expressed by the dependence of the propagation speed of waves on their frequency and direction of propagation. This effect is weaker as the spatial step is small compared to the smallest wavelength λ_{min} of the useful bandwidth. However, this also implies a smaller time step according to the stability relation and thus a longer simulation time. Generally a good trade off consists in taking a spatial step $\Delta_s = \lambda_{min}/10$ [46]. Since TR experiments in reverberant cavities require long simulation times, the numerical dispersion will not be negligible [47]. However, TR can operate in dispersive media, the dispersion being intrinsically compensated by the process [47–49].

For the TE case, density, velocity, and electric field are defined at the same locations, meaning at the corners of the cells. Using a simple explicit scheme, equations (13) and (15) becomes:

$$E_z^{n+1} = \frac{1-\beta}{1+\beta}E_z^n + \frac{en_e\Delta_t}{2\varepsilon_0}\frac{1+\alpha}{1+\beta}v_e^n + \frac{\Delta_t}{\varepsilon_0(1+\beta)}\left(\frac{\partial H_y^{n+1/2}}{\partial x} - \frac{\partial H_x^{n+1/2}}{\partial y}\right) \quad (17)$$

$$v_e^{n+1} = \alpha v_e^n - \frac{e\Delta_t}{2m_e\zeta}\left(E_z^{n+1} + E_z^n\right) \quad (18)$$

with:

$$\alpha = \frac{1-a}{1+a},\ \zeta = 1+a,\ a = \frac{\nu_m\Delta_t}{2} \quad \text{and } \beta = \frac{\omega_p^2\Delta_t^2}{4\zeta} + \frac{\Delta_t}{2\varepsilon_0}\sigma \quad (19)$$

Here, the temporal index 'n' denote the time $t = n\Delta_t$. These equations for electric field and velocity, along with the conventional equation for the magnetic field are stepped in time, alternately updating the electric and magnetic field components at each grid point. We use the same grid spacing, noted Δ_s in the x and y directions, and the time step of the FDTD scheme is $\Delta_t = 0.5\Delta_s/c$, where c is the velocity of light.

Furthermore, equation (16) becomes:

$$n_e^{n+1} = (1 + \Delta_{t_F}\nu_i)\, n_e^n \quad (20)$$

with Δ_{t_F} the time step for the continuity equation, corresponding to the wave period $\Delta_{t_F} = 1/f_c$ [43].

The principle of the algorithm describing the space-time evolution of electromagnetic and plasma quantities is as follows. Maxwell equations (equation (17) with the conventional equations for the magnetic field), together with the electron momentum equation (equation (18)), are solved during one period of the electromagnetic wave. The rms field then calculated is used to solve the density equation at time step Δ_{t_F} (this is possible because the time scale of the density variations is much longer than that of the 2.4 GHz electromagnetic field). Then Maxwell equations and the electron momentum equation are solved over the next period using the updated density. This numerical model is used in the following section for investigating the validity of the "Plasma Steering Criterion".

V. DESCRIPTION OF PLASMA IGNITION BY TIME REVERSAL

In this section, we make use of the model presented in section IV to describe a plasma ignition by TR when the "Plasma Steering Criterion" introduced in section III is respected or not.

The values of the breakdown field, according to equation (6) (using data from Bolsig + and neglecting diffusion), are found to be in our conditions (argon, $p = 1.5$ torr, $f_c = 2.4$ GHz, $\tau = 4$ ns and $\tau_r = 300$ ns):

- $E_b(\tau) \approx 3200$ V/cm
- $E_b(2\tau_r) \approx 180$ V/cm

Thus, we find a condition $SNR > R_b = 18$ that must be respected for an accurate space-time control of plasmas by TR.

The quality of this control is also conditioned by the plasma density. Indeed, the nature of the wave-plasma interaction is a function of the ratio of the carrier frequency f_c and the plasma frequency f_p. The latter is defined as: $f_p = 1/2\pi.\sqrt{n_e e^2/m_e\varepsilon_0}$, with e the electron charge and m_e the electron mass. At low density, meaning for $f_p/f_c << 1 \leftrightarrow n_e << n_{e_c}$ (with n_{e_c} the critical density), the plasma behaves as a dielectric (with a permittivity close to the one of vacuum). In this case the behavior of the waves inside the cavity is not much affected by the presence of plasmas in the cavity. At high density, meaning for $f_p/f_c >> 1 \leftrightarrow n_e >> n_{e_c}$, the plasma behaves as a conductor. In this case the behavior of the waves inside the cavity may significantly be affected by the presence of plasmas in the cavity (for example by reflection of waves by the plasma). In our case (for a central frequency of $f_c = 2.4$ GHz), the critical plasma density from which the behavior of the plasma changes is of $n_{e_c} = 7.10^{16}$ m^{-3}. We will show in this section how this critical density is an important parameter on the plasmas control capabilities of STPSS.

For each simulation presented in this section, the electric field at the focusing location $E_{TR}(t)$ is plotted for two cases: "without plasma" that corresponds to a simulation in which only Maxwell equations are used (no fluid model) and "with plasma" that corresponds to a simulation in which the fluid model is resolved on the part of cavity shown on Figure 4. The temporal evolution of the density $n_{e_{TR}}(t)$ measured at the focusing location is also plotted. Its value $n_{e_{TR}}(\tau_e)$ at the end of the simulation $\tau_e = 600$ ns must be superior to $10^8 n_{e_0}$ for a breakdown to occur at the focusing location.

V.1. "Plasma Steering Criterion" not respected

Experimentally, TR plasmas have been ignited with only one antenna in the TRM [17–19]. In this case (overmoded cavity with $N_{ant} = 1$) the signal-to-noise ratio can be estimated as $SNR = \sqrt{\Delta f/\Gamma}$ [35, 37, 38] and is found to be $SNR = 6.5$. The rms value of the noise before and after the focusing peak, applied during 600 ns, is in this case equal to $E_{noise}^{N_{ant}=1} = E_p/SNR \approx 490$ V/cm. This value is superior to the breakdown field for a duration of 600 ns, which is of $E_b(2\tau_r) \approx 180$ V/cm. In other words, $SNR < R_b$, meaning the "Plasma Steering Criterion" is not respected.

An example of plasma ignition by TR obtained in simulation in those conditions is plotted on Figure 5 with an initial plasma density $n_{e_0} = 10^6$ m^{-3}. This density corresponds to the typical number of free electrons in a metallic chamber (which are caused by cosmic ray) [50, 51]. In this case, a breakdown occurs when the plasma density

has reached 10^{14} m^{-3}, meaning a lower density than the critical plasma density.

The TR focusing peak of duration $\tau = 4$ ns is obtained at $t_p = 300$ ns, with surrounding noise after and before. On the spatial snapshots of the plasma density, the plasma density increases during the focusing, meaning during $\tau = 4$ ns around $t_p = 300$ ns, and at the focusing location, meaning a surface of diameter $\lambda_c/2$ at location $\mathbf{r}_p$. First we note that the signals $E_{TR}(t)$ without and with plasma are very closed to each other. This means that the increase of the plasma density at the focusing location and elsewhere in the cavity does not significantly affects the behavior of the waves. However, there seems to be a change of behavior around 400 ns.

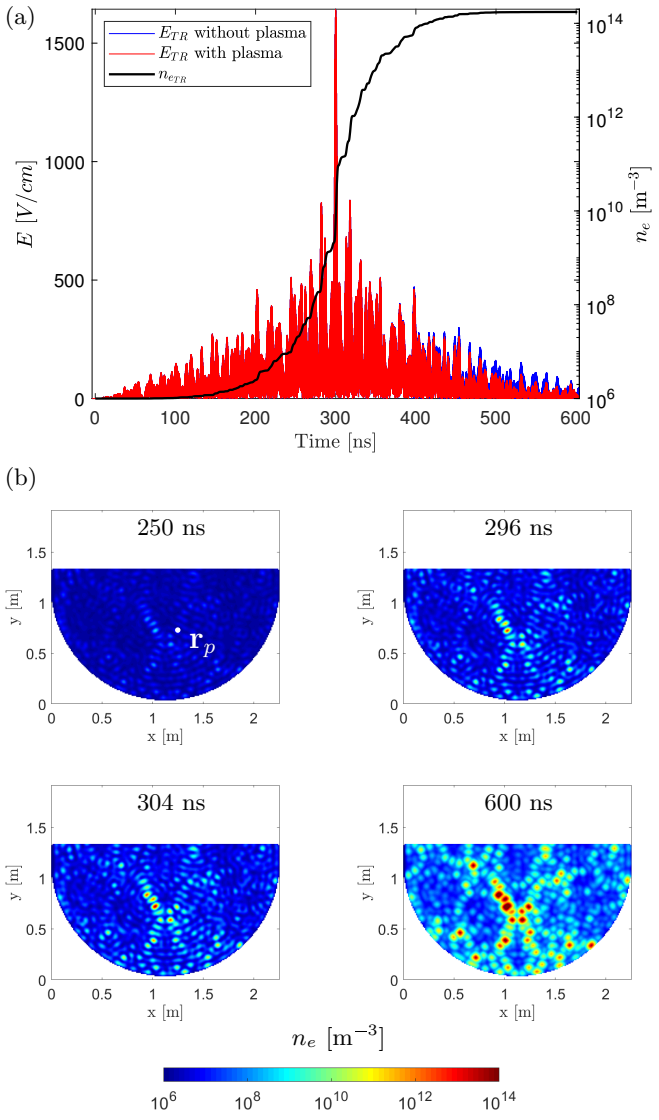

Figure 5. Example of a plasma ignition by TR with an initial plasma density $n_{e_0} = 10^6$ m^{-3} and $N_{ant} = 1$. (a) Electric fields (without and with plasma) and plasma density measured at the focusing location. (b) Snapshots of the plasma density at different instants. Colorbar is settled with a minimal value equal to n_{e_0} and a maximum value of $10^8 n_{e_0}$.

Before 400 ns, the two fields (without and with plasma) have exactly the same temporal shape, with a level slightly lower (not visible on the Figure 5) for the case with plasma due to plasma absorption. This absorption of electromagnetic energy by the plasma leads to an increase of the plasma density at the focusing location as can be seen on the evolution of $n_{e_{TR}}(t)$. This evolution shows the influence of the lobes before and after the focusing peak, which contribute to the majority of the increase of plasma density.

After 400 ns, the evolutions of the two fields differ from one another whereas the density at the focusing location remains much lower than the critical plasma density. This difference comes from the presence of parasitic discharges in the cavity, parasitic discharges that can be seen on the spatial snapshots of the plasma density of Figure 5. Some of these parasitic discharges possess higher density than the one at the focusing location. The location of the parasitic discharge with the highest density is noted as $\mathbf{r}_{par}$. The evolution of the electric fields $E_{par}(t)$ without and with plasma as well as the plasma density $n_{e_{par}}(t)$ at this location are plotted on Figure 6. Even if the maximum level of the field at this location is lower than the level of the focusing peak, a parasitic discharge is generated at this location, with a higher density than the one obtained at the focusing location. The density $n_{e_{par}}(t)$ of this parasitic discharge becomes superior to the critical density n_{e_c} around 400 ns, as represented on Figure 6. This explains the change of behavior of the electric fields without and with plasma around 400 ns at this location. Furthermore, this may also explain the same change of behavior observed at the focusing location on Figure 5. Indeed, the high plasma density at $\mathbf{r}_{par}$ influences the behavior of the wave at this location, thus impacting the behavior of the waves in the cavity and so of the field measured at another location.

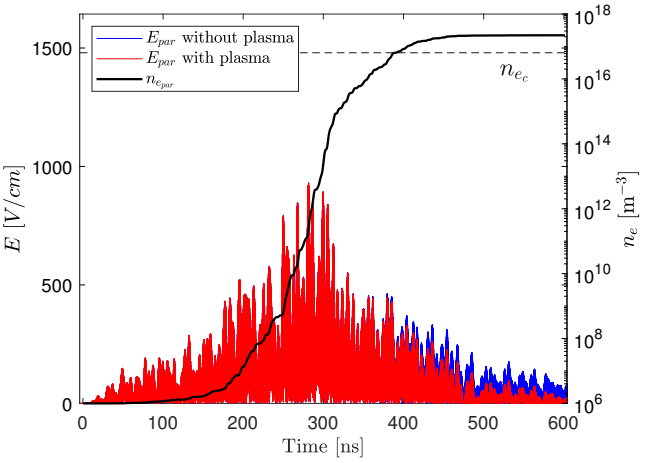

Figure 6. Evolution of the electric fields $E_{par}(t)$ without and with plasma and of the plasma density $n_{e_{par}}(t)$, measured at location $\mathbf{r}_{par}$.

In this case, plasma ignition at the desired location is not possible without the presence of significant parasitic discharges. This supports our claim that when the

"Plasma Steering Criterion" is not respected, parasitic discharges may easily occur and thus space-time control of plasmas by TR is not possible in these conditions[4].

V.2. "Plasma Steering Criterion" respected

As the aim of this paper is to explore the space-time patterning capabilities of the STPSS, we choose to enhance the value of signal-to-noise ratio so that equation (11) is respected. As noted in section III.2, several solutions are possible. In our simulation, the easiest way to enhance the SNR is to increase the number N_{ant} of transmitters in the TRM. Indeed, it does not increase the computation time and it allows to keep similar conditions as the experimental ones (same τ, τ_r, f_c and d). Finally, the number of transducers in the TRM is chosen equal to $N_{ant} = 10$, as it allows to obtain a signal-to-noise ratio $SNR \approx 20.5 > R_b$, meaning the "Plasma Steering Criterion" is respected. It is important to note that although the easiest way to respect the "Plasma Steering Criterion" in our simulations is the increase of the number of antenna in the TRM, in practice it would seem easier to include this criterion in the early design process stages of the system, so that the final system respect this criterion.

Two cases are studied for highlighting the difference of behavior depending on value of the plasma density compared to the critical plasma density. The first case is simulated with an initial plasma density of $n_{e_0} = 10^6$ m^{-3}, leading to a plasma density at the focusing location of 10^{14} m^{-3} inferior to the critical plasma density[5]. The second case is simulated with an initial plasma density of $n_{e_0} = 10^9$ m^{-3}, leading to a plasma density at the focusing location of 10^{17} m^{-3} superior to the critical plasma density.

V.2.1. Time Reversal plasma density inferior to the critical plasma density

Plasma ignition by TR with $N_{ant} = 10$ at the same location as the one that has been previously chosen with $N_{ant} = 1$ and the same initial plasma density $n_{e_0} = 10^6$ m^{-3} is plotted on Figure 7.

In this case, the focusing peak is responsible for an increase of 10^4 on the plasma density, so half of its total logarithmic increase during the TR operation. On the snapshots of plasma density, we can clearly see a plasma ignited only at the focusing location $\mathbf{r}_p$, on a surface of diameter $\lambda_c/2$. The density obtained at the focusing is superior to the one obtained anywhere in the cavity, reflecting the successful ignition of plasma by TR. We see the presence of secondary lobes of plasma density, which possess on average densities lower by a factor 10^4 (with the highest secondary lobes lower by a factor 10^3).

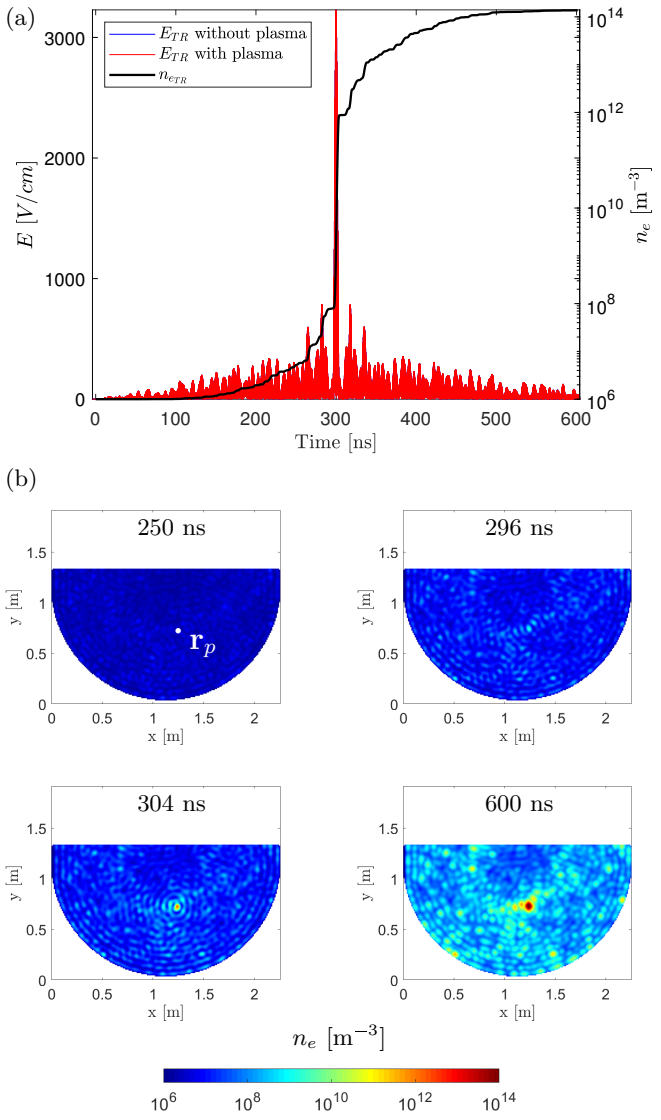

Figure 7. Example of a plasma ignition by TR with an initial plasma density $n_{e_0} = 10^6$ m^{-3} and $N_{ant} = 10$. (a) Electric fields (without and with plasma) and plasma density measured at the focusing location. (b) Snapshots of the plasma density at different instants. Colorbar is settled with a minimal value equal to n_{e_0} and a maximum value of $10^8 n_{e_0}$.

The signals $E_{TR}(t)$ without and with plasma are closed to each other during the whole TR operation. As for previous results with $N_{ant} = 1$, the one with plasma is slightly lower than the one without (this difference is not visible on Figure 7), due to plasma absorption. This similarity of the waveforms of $E_{TR}(t)$ without and with plasma is due to the fact that the plasma density

[4] Experimentally, plasmas have been successfully controlled by TR in those conditions [17, 18]. However, in the experiments theses plasmas have been ignited on initiators, which locally enhance the electric field, limiting the possibility of generating parasitic discharges in the cavity.

[5] Note that in practice, a density of 10^{14} m^{-3} is quite low for a plasma. However, similar behavior is obtained with higher plasma densities at the focusing location as long as they remains lower than the critical plasma density (for example with initial plasma densities of 10^7 m^{-3} and 10^8 m^{-3}, leading to plasma density at the focusing location of 10^{15} m^{-3} and 10^{16} m^{-3}).

anywhere in the cavity is lower than the critical plasma density.

Horizontal and vertical cuts at the focusing location are plotted, at the focusing instant (300 ns) for the electric field and right after (304 ns) for the plasma density, on Figure 8. Snapshots of the electric field and of the plasma density are also plotted at these instants.

The snapshot of the electric field shows the focusing of the waves at the focusing location, of dimension $\lambda_c/2$ (as predicted in [44]). However, this focusing lasts $\tau = 4$ ns and is modulated by a carrier frequency of $f_c = 2.4$ GHz. At the location of focusing, the field will therefore oscillate at 2.4 GHz during 4 ns on a dimension of 6 cm. This is why we see, around the focusing peak, cylindrical wavefronts converging towards the focusing point (since the focusing will still last 4 ns). Their cylindrical shape is a consequence of the chaoticity of the cavity, that allows to recreate cylindrical wavefronts since the waves arrive from all directions [36].

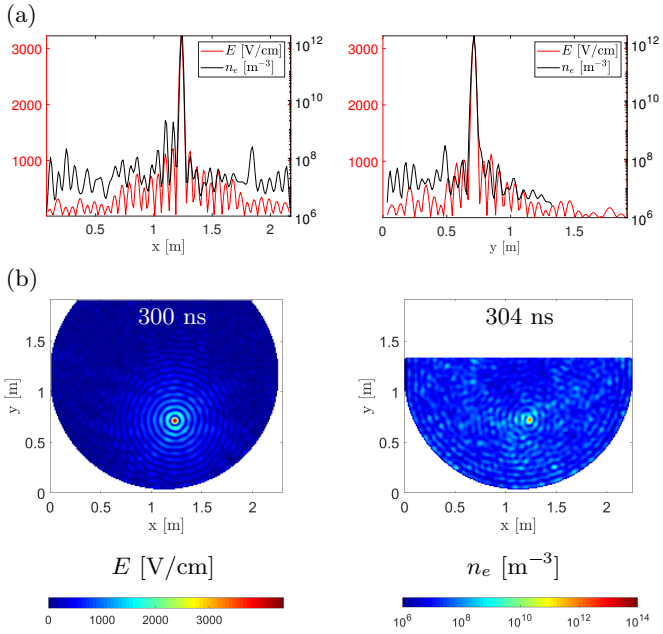

Figure 8. Focus on the TR focusing with an initial plasma density $n_{e_0} = 10^6$ m^{-3}. (a) Horizontal and vertical cuts at the focusing location, meaning along the x axis for $y = 0.7$ m and along the y axis for $x = 1.2$ m, respectively. In red is plotted the electric field at the focusing instant $t = 300$ ns and in black is plotted the plasma density right after the focusing peak at $t = 304$ ns. (b) Snapshots of the electric field and plasma density at these instants (meaning $t = 300$ ns and $t = 304$ ns, respectively).

The snapshot of the plasma density shows a dimension of the plasma obtained at the focusing similar to the one of the focusing, with relatively high secondary lobes around the focusing due to the high level of the field of cylindrical wavefronts shown on the snapshot of the electric field. On the horizontal and vertical cuts plotted on Figure 8, it is clear that the shape of the plasma ignited by TR is determined by the shape of the TR focusing pulse. Thus, plasmas ignited by TR are found to have a dimension at half maximum of $\lambda_c/2 \approx 6$ cm.

V.2.2. Time Reversal plasma density superior to the critical plasma density

To highlight the influence of the plasma density on the plasma control capabilities of STPSS, plasma ignition by TR with $N_{ant} = 10$ at the same location as the one that has been previously chosen and with an initial plasma density $n_{e_0} = 10^9$ m^{-3} is plotted on Figure 9.

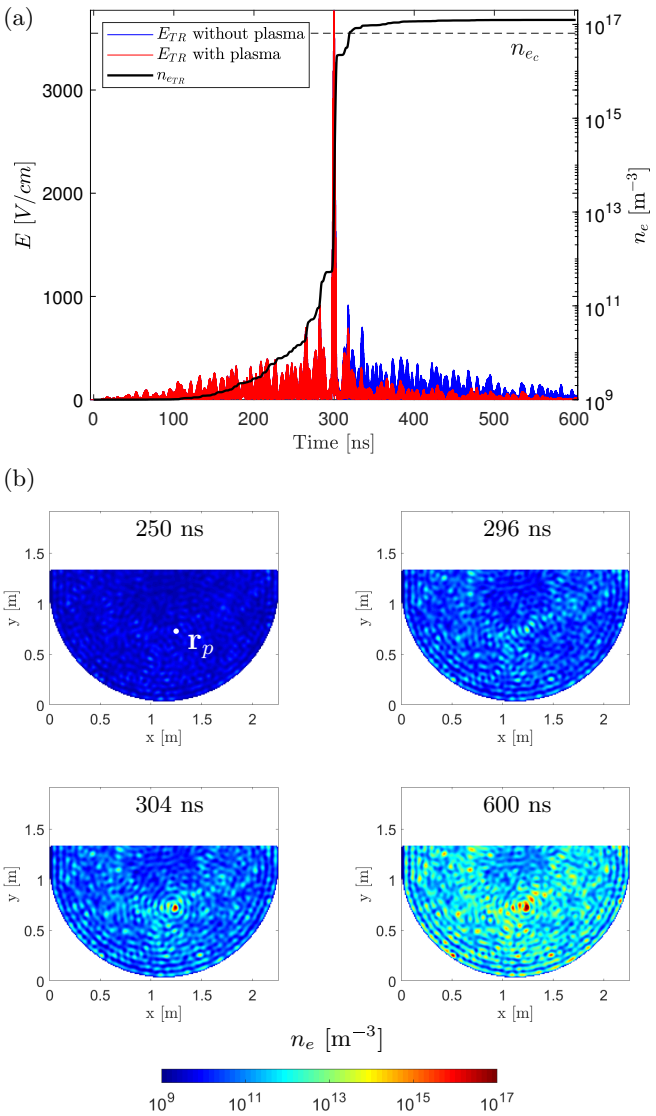

Figure 9. Example of a plasma ignition by TR with an initial plasma density $n_{e_0} = 10^9$ m^{-3} and $N_{ant} = 10$. (a) Electric fields (without and with plasma) and plasma density measured at the focusing location. (b) Snapshots of the plasma density at different instants. Colorbar is settled with a minimal value equal to n_{e_0} and a maximum value of $10^8 n_{e_0}$.

In this case the signals $E_{TR}(t)$ without and with plasma are close to each other before and during the focusing peak. After the focusing peak, the $E_{TR}(t)$ with

plasma is lower than the one without plasma. The focusing peak is responsible for an increase of more than 10^4 on the plasma density, so more than half of its total logarithmic increase during the TR operation. On the snapshots of plasma density, we can clearly see a plasma ignited only at the focusing location $\mathbf{r}_p$, on a surface of diameter $\lambda_c/2$. The density obtained at the focusing is superior to the one obtained anywhere in the cavity, reflecting the successful ignition of plasma by TR. We see the presence of secondary lobes of plasma density, which possess on average densities lower by a factor 10^4.

However, contrary to the previous case with an initial density of $n_{e_0} = 10^6$ m^{-3}, the secondary lobes with the highest densities possess relatively high densities, of about 10^{15} m^{-3}. This is due to the reflection of the waves by the plasma at the focusing location. Indeed, as shown on Figure 9, the plasma density at the focusing location becomes greater than the critical plasma density around 320 ns. The waves are thus reflected by the plasma at this location and a lower field level is obtained compared to the case without plasma. After this instant, the increase of the plasma density is lower than in the previous case (for an initial density of $n_{e_0} = 10^6$ m^{-3}) in which the waves where not reflected by the plasma and could thus play a more significant role on the increase of the plasma density (Figure 7). This is why the level of focusing field with an initial density of $n_{e_0} = 10^9$ m^{-3} required for an increase of a factor 10^8 is higher than the one required with an initial density of $n_{e_0} = 10^6$ m^{-3}. This leads to secondary lobes of density with higher densities.

V.2.3. Synthesis

In both cases, meaning for initial density of $n_{e_0} = 10^6$ m^{-3} and $n_{e_0} = 10^9$ m^{-3}, the control of plasma by TR is effective. This supports our claim that when the "Plasma Steering Criterion" is respected, parasitic discharges are avoided and thus space-time control of plasmas by TR is possible. However, plasma density obtained at the focusing location also plays a role on the control capabilities of STPSS, depending on its value with respect to the critical plasma density.

Furthermore, a thorough attention is required on this last point when a pulsed regime will be considered. Indeed, when the plasma density is close to or superior to the critical plasma density, its presence in the cavity may change its fundamental characteristics, modifying the resonant modes. Thus, if the density of a previous peak is still close to or superior to the critical plasma density at the next iteration, the behavior of the waves may be significantly affected, resulting in a degradation of the focusing capabilities.

Thus, controlling plasmas of high density (close to the critical density) may require more advanced techniques, that allows the nonlinear behavior of these plasmas to be taken into account. To that end, TR may still offers promising outlooks, as it has been extended to electromagnetic cavities containing nonlinearity [52, 53]. Furthermore, other methods that have recently been developed [54], which allow the control of electromagnetic fields in nonlinear systems, also seems to be promising for the space-time control of these nonlinear plasmas.

VI. CONCLUSION

Space-Time Plasma Steering Source has been introduced to meet the challenge of controlling plasmas in large, overmoded cavities. This original plasma source may find applications in the context of surface processing, as it could lead the development of plasma assisted processing and tool manufacturing. Space-Time Plasma Steering Source could also find applications in the context of "Space-time modulated media" [55]. It has received recently a notable interest in the context of electromagnetic wave engineering, as it allow the development of materials with exotic and unique properties [55, 56]. In particular, space-time metamaterials [57–59] have received a lot of attention. Space-time control of 3D plasma patterns by STPSS could lead to promising applications in this domain.

The control of energy deposition in time and space also offers new opportunities to study and control microwave plasma breakdown. Indeed, the control of the electromagnetic energy deposition on dimensions inferiors to the ones of the breakdown pattern and on durations inferiors to the breakdown dynamics could lead to unprecedented control of these breakdown pattern and dynamics. Furthermore, field polarization has also been shown to have a significant impact on microwave breakdown dynamics and pattern [60]. Although it was not discussed in this paper, TR allows the control of the focusing field polarization [61, 62]. Thus, this Space-Time Plasma Steering Source could lead to the development of methods allowing the space-time sculpture of microwave breakdown, with the microwave energy that would "accompany" the breakdown dynamics and pattern.

Experimentally, the most essential step that needs to be taken for the development of this innovative plasma source is the "unhooking" of the plasmas from the initiators [20]. This paper gives insights into the path that shall be taken to reach this objective. To that end, a key criterion, namely the "Plasma Steering criterion", is introduced. It must be respected for an accurate control of plasmas in overmoded cavities. The validity of this criterion is verified in the case of STPSS based on TR with a numerical model. When this criterion is not respected, several solutions are possibles and discussed in this paper. The influence of the plasma density obtained at the focusing location (depending on its value with respect to the critical plasma density) on the plasma control capabilities is also highlighted.

ACKNOWLEDGMENTS

The authors want to acknowledge the DGA/AID for their funding support.

[1] S. Samukawa, M. Hori, S. Rauf, K. Tachibana, P. Bruggeman, G. Kroesen, J. C. Whitehead, A. B. Murphy, A. F. Gutsol, S. Starikovskaia, U. Kortshagen, J.-P. Boeuf, T. J. Sommerer, M. J. Kushner, U. Czarnetzki, and N. Mason, The 2012 Plasma Roadmap, J. Phys. D: Appl. Phys. **45**, 253001 (2012).

[2] T. H. Chang, N. C. Chen, H. W. Chao, J. C. Lin, C. C. Huang, and C. C. Chen, Generating large-area uniform microwave field for plasma excitation, Physics of Plasmas **19**, 033302 (2012).

[3] D. Korzec, F. Hoppenthaler, A. Shestakov, D. Burger, A. Shapiro, T. Andres, S. Lerach, and S. Nettesheim, Multi-Device Piezoelectric Direct Discharge for Large Area Plasma Treatment, Plasma **4**, 281 (2021).

[4] D. Korzec, F. Werner, R. Winter, and J. Engemann, Scaling of microwave slot antenna (SLAN): a concept for efficient plasma generation, Plasma Sources Sci. Technol. **5**, 216 (1996).

[5] D. Korzec, M. Mildner, F. Hillemann, and J. Engemann, 70cm radio frequency hollow cathode plasma source for modification of foils and membranes, Surface and Coatings Technology **97**, 759 (1997).

[6] J. Engemann and D. Korzec, Assessment of discharges for large area atmospheric pressure plasma-enhanced chemical vapor deposition (AP PE-CVD), Thin Solid Films **442**, 36 (2003).

[7] B. D. Gates, Nanofabrication with molds & stamps, Materials Today **8**, 44 (2005).

[8] D.-Y. Kang, W. Lee, D. Kim, and J. H. Moon, Three-Dimensional Polymeric Mechanical Metamaterials Fabricated by Multibeam Interference Lithography with the Assistance of Plasma Etching, Langmuir **32**, 8436 (2016).

[9] O. Baranov, K. Bazaka, H. Kersten, M. Keidar, U. Cvelbar, S. Xu, and I. Levchenko, Plasma under control: Advanced solutions and perspectives for plasma flux management in material treatment and nanosynthesis, Applied Physics Reviews **4**, 041302 (2017).

[10] Y.-X. Liu, Y.-R. Zhang, A. Bogaerts, and Y.-N. Wang, Electromagnetic effects in high-frequency large-area capacitive discharges: A review, Journal of Vacuum Science & Technology A **33**, 020801 (2015).

[11] M. A. Lieberman, J. P. Booth, P. Chabert, J. M. Rax, and M. M. Turner, Standing wave and skin effects in large-area, high-frequency capacitive discharges, Plasma Sources Sci. Technol. **11**, 283 (2002).

[12] G. S. J. Sturm, M. D. Verweij, A. I. Stankiewicz, and G. D. Stefanidis, Microwaves and microreactors: Design challenges and remedies, Chemical Engineering Journal **243**, 147 (2014).

[13] H. Kim and J. Hopwood, Wave Propagation in Composites of Plasma and Metamaterials with Negative Permittivity and Permeability, Sci Rep **9**, 3024 (2019).

[14] R. Navarro, L. Liard, and J. Sokoloff, Effects of a low pressure plasma on a negative-permeability metamaterial, Journal of Applied Physics **126**, 163304 (2019).

[15] J. A. Rodriguez, A. I. Abdalla, B. Wang, B. Lou, S. Fan, and M. A. Cappelli, Inverse Design of Plasma Metamaterial Devices for Optical Computing, Phys. Rev. Applied **16**, 014023 (2021).

[16] O. Sakai and K. Tachibana, Plasmas as metamaterials: a review, Plasma Sources Sci. Technol. **21**, 013001 (2012).

[17] V. Mazières, R. Pascaud, L. Liard, S. Dap, R. Clergereaux, and O. Pascal, Plasma generation using time reversal of microwaves, Appl. Phys. Lett. **115**, 154101 (2019).

[18] V. Mazières, R. Pascaud, O. Pascal, R. Clergereaux, L. Stafford, S. Dap, and L. Liard, Spatio-temporal dynamics of a nanosecond pulsed microwave plasma ignited by time reversal, Plasma Sources Sci. Technol. **29**, 125017 (2020).

[19] V. Mazières, A. A. Ibrahim, C. Chauvière, P. Bonnet, R. Pascaud, R. Clergereaux, S. Dap, L. Liard, and O. Pascal, Transient Electric Field Shaping With the Linear Combination of Configuration Field Method for Enhanced Spatial Control of Microwave Plasmas, IEEE Access **8**, 177084 (2020).

[20] V. Mazières, R. Pascaud, L. Stafford, P. Bonnet, A. Al Ibrahim, C. Chauvière, L. Liard, S. Dap, R. Clergereaux, and O. Pascal, Space-Time Plasma Steering Source: Synthesis and Outlooks, in *2021 XXXIVth General Assembly and Scientific Symposium of the International Union of Radio Science (URSI GASS)* (2021) pp. 1–4, iSSN: 2642-4339.

[21] K. Chang, ed., *Encyclopedia of RF and Microwave Engineering , 6-Volume Set*, 1st ed. (Wiley-Interscience, Hoboken, N.J, 2005).

[22] A. Cozza, Statistics of the performance of time reversal in a lossy reverberating medium, Phys. Rev. E **80**, 056604 (2009).

[23] A. Cozza and F. Monsef, Multiple-Source Time-Reversal Transmissions in Random Media, IEEE Transactions on Antennas and Propagation **62**, 4269 (2014).

[24] E. I. GREEN, THE STORY OF Q, American Scientist **43**, 584 (1955).

[25] F. Monsef and A. Cozza, Average Number of Significant Modes Excited in a Mode-Stirred Reverberation Chamber, IEEE Transactions on Electromagnetic Compatibility **56**, 259 (2014).

[26] J. J. Su, Y. F. Li, X. L. Li, P. L. Yao, Y. Q. Liu, M. H. Ding, and W. Z. Tang, A novel microwave plasma reactor with a unique structure for chemical vapor deposition of diamond films, Diamond and Related Materials **42**, 28 (2014).

[27] J. Weng, L. W. Xiong, J. H. Wang, S. Y. Dai, W. D. Man, and F. Liu, Investigation of depositing large area uniform diamond films in multi-mode MPCVD chamber, Diamond and Related Materials **30**, 15 (2012).

[28] A. L. Vikharev, A. M. Gorbachev, M. A. Lobaev, and D. B. Radishev, Multimode cavity type MPACVD reactor for large area diamond film deposition, Diamond and Related Materials **83**, 8 (2018).

[29] J. Weng, J. H. Wang, S. Y. Dai, L. W. Xiong, W. D.

Man, and F. Liu, Preparation of diamond films with controllable surface morphology, orientation and quality in an overmoded microwave plasma CVD chamber, Applied Surface Science **276**, 529 (2013).
[30] L. Gould and L. W. Roberts, Breakdown of Air at Microwave Frequencies, Journal of Applied Physics **27**, 1162 (1956).
[31] U. Jordan, D. Anderson, M. Backstrom, A. Kim, M. Lisak, and O. Lunden, Microwave breakdown in slots, IEEE Transactions on Plasma Science **32**, 2250 (2004).
[32] P. Felsenthal, Nanosecond-Pulse Microwave Breakdown in Air, Journal of Applied Physics **37**, 4557 (1966).
[33] P.-C. Zhao, C. Liao, and J. Feng, Short-pulse high-power microwave breakdown at high pressures, Chinese Physics B **24**, 025101 (2015).
[34] C. Caloz, A. Alu, S. Tretyakov, D. Sounas, K. Achouri, and Z.-L. Deck-Leger, Electromagnetic Nonreciprocity, Phys. Rev. Applied **10**, 047001 (2018).
[35] A. Derode, A. Tourin, and M. Fink, Random multiple scattering of ultrasound. II. Is time reversal a self-averaging process?, Phys. Rev. E **64**, 036606 (2001).
[36] C. Draeger, J.-C. Aime, and M. Fink, One-channel time-reversal in chaotic cavities: Experimental results, The Journal of the Acoustical Society of America **105**, 618 (1999).
[37] A. Derode, A. Tourin, and M. Fink, Limits of time-reversal focusing through multiple scattering: Long-range correlation, The Journal of the Acoustical Society of America **107**, 2987 (2000).
[38] J. d. Rosny, *Milieux réverbérants et réversibilité*, These de doctorat, Paris 6 (2000).
[39] H. Moussa, A. Cozza, and M. Cauteman, A novel way of using reverberation chambers through time reversal, in *ESA Workshop on Aerospace EMC (ESA'09)* (Italy, 2009) pp. 10–2.
[40] I. El Baba, S. Lalléchère, and P. Bonnet, Time Reversal for Electromagnetism: Applications in Electromagnetic Compatibility, Trends in Electromagnetism - From Fundamentals to Applications (2012).
[41] M. Fink, C. Prada, F. Wu, and D. Cassereau, Self focusing in inhomogeneous media with time reversal acoustic mirrors, in *Proceedings., IEEE Ultrasonics Symposium,* (1989) pp. 681–686 vol.2.
[42] J.-P. Boeuf, B. Chaudhury, and G. Q. Zhu, Theory and Modeling of Self-Organization and Propagation of Filamentary Plasma Arrays in Microwave Breakdown at Atmospheric Pressure, Phys. Rev. Lett. **104**, 015002 (2010).
[43] B. Chaudhury and J.-P. Boeuf, Computational Studies of Filamentary Pattern Formation in a High Power Microwave Breakdown Generated Air Plasma, IEEE Transactions on Plasma Science **38**, 2281 (2010).
[44] G. Lerosey, J. de Rosny, A. Tourin, A. Derode, G. Montaldo, and M. Fink, Time Reversal of Electromagnetic Waves, Phys. Rev. Lett. **92**, 193904 (2004).
[45] G. J. M. Hagelaar and L. C. Pitchford, Solving the Boltzmann equation to obtain electron transport coefficients and rate coefficients for fluid models, Plasma Sources Sci. Technol. **14**, 722 (2005).
[46] A. Taflove and S. Hagness, *Computational Electrodynamics: The Finite-Difference Time-Domain Method*, 3rd ed. (Artech House Publishers, Boston, 2005).
[47] C. Draeger and M. Fink, One-channel time-reversal in chaotic cavities: Theoretical limits, The Journal of the Acoustical Society of America **105**, 611 (1999).
[48] R. Ernst and J. Dual, Quantitative guided wave testing by applying the time reversal principle on dispersive waves in beams, Wave Motion **58**, 259 (2015).
[49] H. W. Park, S. B. Kim, and H. Sohn, Understanding a time reversal process in Lamb wave propagation, Wave Motion **46**, 451 (2009).
[50] S. Pancheshnyi, Role of electronegative gas admixtures in streamer start, propagation and branching phenomena, Plasma Sources Sci. Technol. **14**, 645 (2005).
[51] M. Ghassemi, H. Mohseni, K. Niayesh, and A. A. Shayegani, A detailed model for discharge initiation in argon at atmospheric pressure in presence of dielectric barriers, IEEE Transactions on Dielectrics and Electrical Insulation **19**, 865 (2012).
[52] S. K. Hong, V. M. Mendez, T. Koch, W. S. Wall, and S. M. Anlage, Nonlinear Electromagnetic Time Reversal in an Open Semireverberant System, Phys. Rev. Applied **2**, 044013 (2014).
[53] M. Frazier, B. Taddese, T. Antonsen, and S. M. Anlage, Nonlinear Time Reversal in a Wave Chaotic System, Phys. Rev. Lett. **110**, 063902 (2013).
[54] A. Al Ibrahim, C. Chauvière, and P. Bonnet, Time-Domain Software Correction of Nonlinear Faulty Lossy Transmission Line Networks, IEEE Transactions on Electromagnetic Compatibility **62**, 1304 (2020).
[55] S. Taravati and A. A. Kishk, Space-Time Modulation: Principles and Applications, IEEE Microwave Magazine **21**, 30 (2020).
[56] S. Taravati, Giant Linear Nonreciprocity, Zero Reflection, and Zero Band Gap in Equilibrated Space-Time-Varying Media, Phys. Rev. Applied **9**, 064012 (2018).
[57] P.A. Huidobro, M.G. Silveirinha, E. Galiffi, and J.B. Pendry, Homogenization Theory of Space-Time Metamaterials, Phys. Rev. Applied **16**, 014044 (2021).
[58] C. Caloz and Z.-L. Deck-Leger, Spacetime Metamaterials—Part I: General Concepts, IEEE Transactions on Antennas and Propagation **68**, 1569 (2020).
[59] C. Caloz and Z.-L. Deck-Leger, Spacetime Metamaterials—Part II: Theory and Applications, IEEE Transactions on Antennas and Propagation **68**, 1583 (2020).
[60] K. Kourtzanidis, J. P. Boeuf, and F. Rogier, Three dimensional simulations of pattern formation during high-pressure, freely localized microwave breakdown in air, Physics of Plasmas **21**, 123513 (2014).
[61] D. A. M. Iero, L. Crocco, and T. Isernia, On the Role and Choice of Source Polarization in Time-Reversal Focusing of Vector Fields, IEEE Antennas and Wireless Propagation Letters **15**, 214 (2016).
[62] D. a. M. Iero, L. Crocco, and T. Isernia, Advances in 3-D electromagnetic focusing: Optimized time reversal and optimal constrained power focusing, Radio Science **52**, 166 (2017).